The Electronic Structure of Highly Anisotropic Low-Spin Ferric Porphyrin Complexes Based on Single-Crystal EPR Measurements

Daryl Inniss, S. Michael Soltis, and Charles E. Strouse*

Contribution from the Department of Chemistry and Biochemistry, the J. D. McCullough X-ray Crystallography Laboratory, and the Solid Science Center, University of California, Los Angeles, California 90024. *Received October 6, 1987*

Abstract: Single-crystal electron spin resonance **g** tensor determinations are reported for three low-spin ferric porphyrin complexes, $[Fe(TPP)(py)_2]ClO_4 \cdot 2THF$, $K[Fe(TPP)(CN)_2] \cdot 2$acetone, and $Fe(TPP)(CN)(py) \cdot H_2O$, all of which exhibit "highly anisotropic low-spin" EPR spectra. These single-crystal measurements allow accurate extraction of the complete **g** tensor, which in turn provides estimates of the wave functions and relative energies of the three highest occupied molecular orbitals. It is the near-degeneracy of the "d_{xz}" and "d_{yz}" orbitals in these complexes that is responsible for the large g value anisotropy; this near-degeneracy has a number of additional consequences. Analysis of the crystal field parameters, derived from the EPR measurements, indicates that for the $(py)_2$ and $(CN)_2$ complexes the product of the three principal g values is negative, whereas for "normal" ferric porphyrin complexes this product is positive. The spin in these complexes is delocalized over the two out-of-plane real d orbitals, whereas in "normal" complexes it is localized in a single real d orbital. For ferric porphyrin complexes with planar axial ligands, this delocalization is associated with a spin–orbit stabilization of the perpendicular ligand conformation. In the case of weak π donors, this stabilization can exceed the crystal field stabilization of the parallel geometry. A crystal structure determination for $[Fe(TPP)(py)_2]ClO_4 \cdot 2THF$ at 128 K reveals that the axial pyridine ligands adopt a perpendicular conformation that is staggered with respect to the equatorial Fe–N(pyrrole) vectors. The idealized S_4 symmetry about the iron center is consistent with the spectroscopic observations. Crystal data: $[Fe(TPP)(py)_2]ClO_4 \cdot 2THF$, space group $A2/a$, $Z = 8$, $a = 22.814$ (2) Å, $b = 17.010$ (2) Å, $c = 27.423$ (2) Å, $\beta = 102.51$ (1)°, at 128 K.

A number of heme proteins and small-molecule ferric porphyrin complexes have been found to exhibit what have been referred to as "highly anisotropic low-spin" (HALS) or "large g_{max}" signals.[1-15] These signals are broad even at low temperatures and are normally undetectable above about 80 K. Analyses of these signals have been difficult because in many cases only the value of g_{max} can be reliably extracted from polycrystalline or frozen solution spectra. Large line widths, the presence of impurities, and the fact that the spectra often extend beyond the range of commercial EPR spectrometers obscure the features associated with the other two principal values. Single-crystal **g** tensor determination can be used to overcome these limitations while providing a direct determination of the orientation of the principal axes of the **g** tensor with respect to the molecular axes. The investigation reported herein includes single-crystal EPR analyses of bis(pyridine), bis(cyanide), and cyano pyridine ferric TPP complexes,[16] which all display highly anisotropic EPR spectra. Structural data for the $(CN)_2$ complex and the (CN)(py) complex have been previously reported by Scheidt, Hatano, and coworkers.[17,18] The structural analysis of the $(py)_2$ complex is reported herein.

Table I. Crystallographic Parameters for $[Fe(TPP)(py)_2]ClO_4 \cdot 2THF$ at 128 K

a, Å	22.841 (2)
b, Å	17.010 (2)
c, Å	27.423 (2)
α, deg	90.000
β, deg	102.51 (1)
γ, deg	90.000
v, Å^3	10391
crystal size, mm	0.19 × 0.22 × 0.38
2θ max, deg	50
Z	8
space group	$A2/a$
tot reflcns	18296
obsd reflcns	9454 (3σ)
parameters refined	594
diffractometer[a]	Picker
R	0.093
R_w	0.109
EOF	2.518

[a] Graphite monochromatized Mo Kα radiation.

In a recent study, Walker, Huynh, Scheidt, and Osvath[1] associated the presence of the HALS spectrum with the perpendicular orientation of planar axial ligands. This geometry should result in a near degeneracy of the iron d_{yz} and d_{xz} orbitals which in turn accounts for the large observed value of g_z. It will be shown that this degeneracy has several additional consequences that must be taken into consideration in the comparison of the electronic and structural parameters of these species with those of "normal" porphyrin complexes.

Experimental Section

Synthesis. Fe(TPP)Cl was used as purchased from Midcentury. Pyridine (py) and tetrahydrofuran (THF) were purchased from Fisher and were used without purification. $[Fe(TPP)(H_2O)_2]ClO_4 \cdot 2THF$ was

(1) Walker, F. A.; Huynh, B. H.; Scheidt, W. R.; Osvath, S. R. *J. Am. Chem. Soc.* **1986**, *108*, 5288.
(2) Gadsby, M. A.; Thomson, A. J. *FEBS* **1986**, *197*, 253.
(3) Babcock, G. T.; Widger, W. R.; Cramer, W. A.; Oertlig, W. A.; Metz, J. G. *Biochemistry* **1985**, *24*, 3638.
(4) Walker, F. A.; Reis, D.; Balke, V. L. *J. Am. Chem. Soc.* **1984**, *106*, 6888.
(5) Salerno, J. C.; Leigh, J. S. *J. Am. Chem. Soc.* **1984**, *106*, 2156.
(6) Salerno, J. C. *J. Biol. Chem.* **1984**, *259*, 2331.
(7) Salerno, J. C.; McGill, J. W.; Gerstle, G. C. *FEBS* **1983**, *162*, 257.
(8) Tsai, A.; Palmer, G. *Biochem. Biophys. Acta* **1982**, *681*, 484.
(9) Migita, C. T.; Iwaizumi, M. *J. Am. Chem. Soc.* **1981**, *103*, 4378.
(10) Carter, K. R.; Tsai, A.; Palmer, G. *FEBS Lett.* **1981**, *132*, 243.
(11) Malkin, R.; Vangard, T. *FEBS Lett.* **1980**, *111*, 218.
(12) Leigh, J. S.; Erecinska, M. *Biochim. Biophys. Acta* **1975**, *387*, 95.
(13) Leigh, J. S.; Erecinska, M. *J. Biol. Chem.* **1974**, *249*, 1928.
(14) Orme-Johnson, N. R.; Hansen, R. E.; Beinert, H. *Biochem. Biophys. Res. Commun.* **1971**, *45*, 871.
(15) Hori, H. *Biochim. Biophys. Acta* **1971**, *251*, 227.
(16) Abbreviations are as follows: $(py)_2$, $[Fe(TPP)(py)_2]ClO_4 \cdot 2THF$; $(CN)_2$, $[Fe(TPP)(CN)_2]K \cdot 2CH_3COCH_3$; (CN)(py), $Fe(TPP)(CN)(py) \cdot H_2O$; TPP, tetraphenylporphinato; PPIX, protoporphyrin IX; py, pyridine; THF, tetrahydrofuran; EPR, electron paramagnetic resonance.
(17) Scheidt, W. R.; Haller, K. J.; Hatano, K. *J. Am. Chem. Soc.* **1980**, *102*, 3017.
(18) Scheidt, W. R.; Lee, Y. J.; Luangdilok; Haller, K. J.; Anzai, K.; Hatano, K. *Inorg. Chem.* **1983**, *22*, 1516.

0002-7863/88/1510-5644$01.50/0

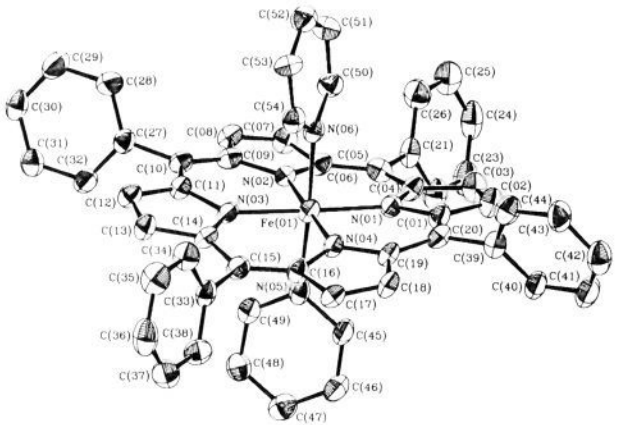

Figure 1. An ORTEP drawing displaying the structure and numbering system for the $[Fe(TPP)(py)_2]$ cation.

prepared from Fe(TPP)Cl and silver perchlorate as described by Scheidt et al.[19] $[Fe(TPP)(py)_2]ClO_4 \cdot 2THF$ was prepared by dissolution of 40 mg of $[Fe(TPP)(H_2O)_2]ClO_4 \cdot 2THF$ in 5 mL of THF. Approximately 6 equiv of pyridine (0.04 mL) and 2 μL of (70%) $HClO_4$ were added and the mixture was stirred for 1 h. After evaporation to a volume of 4 mL, heptane vapor diffusion afforded purple crystals suitable for single-crystal X-ray and EPR analysis. The yield was approximately 90%. Anal. Calcd for $FeClO_6N_6C_{62}H_{54}$: C, 69.66; H, 5.06; N, 7.94. Found: C, 69.56; H, 5.08; N, 7.79. **Caution!** Perchlorates are shock sensitive and can be explosive. Several iron porphyrin perchlorates prepared in this laboratory were found to denonate spontaneously at 200 °C. $K[Fe(TPP)(CN)_2] \cdot 2(CO(CH_3)_2)$ and $Fe(TPP)(CN)(py) \cdot H_2O$ were originally prepared by Scheidt, Hatano, and co-workers.[17,18] Crystals suitable for single-crystal EPR and X-ray characterization were prepared as described by these authors.

Structural Analysis of $[Fe(TPP)(py)_2]ClO_4 \cdot 2THF$. The structural analysis was performed on data collected at 128 K. Attempts to collect data at temperatures below 80 K resulted in fracture of the crystals. Lattice parameters and data collection parameters can be found in Table I.[20] A single crystal was coated with epoxy immediately upon removal from the mother liquor and mounted directly on a glass fiber. Preliminary examination established a monoclinic unit cell.

A linear decay correction of 10% was applied to the intensity data. The structure was solved by heavy atom methods. The Patterson map was interpreted to provide both the iron atom and chlorine atom positions. Subsequent cycles of difference-Fourier synthesis yielded the remaining non-hydrogen atoms. The perchlorate anion was found to be 2-fold disordered and was successfully modeled with the two perchlorate entities refined as separate rigid groups. Both THF solvate molecules were found to be disordered; this disorder was difficult to model. The THF molecule in one site was modeled with a planar 5-membered ring. The second site was modeled with two such rings, each with 0.5 occupancy. The large thermal parameters obtained for these groups reflect the nonplanarity of the THF molecules and possible additional disorder. For all other atoms, both the coordinates and anisotropic temperature factors were well-behaved in the least-squares refinement. All hydrogen atom positions were calculated (C–H = 1.00 Å) and their temperature factors were set to 3.0 Å.[2] In the final refinement the non-hydrogen positions and isotropic temperature factors were refined along with the position, orientation, and isotropic temperature factor for each perchlorate and THF group. Final residuals of $R = 0.093$ and $R_w = 0.109$ were obtained.[21]

(19) Scheidt, W. R.; Cohen, I. A.; Kastner, M. E. *Biochemistry* **1979**, *18*, 3546.

(20) The programs used in this work included modified versions of the following programs: REDUCE (Broach, Coppens, Becker, and Blessing), peak profile analysis, Lorentz and polarization corrections; MULTAN (Main), package of programs, including direct methods, structure factor normalization, Fourier transform, and peak search; ORFLS (Busing, Martin, and Levy), structure factor calculation and full-matrix least-squares refinement; ORFFE (Busing, Martin, and Levy), distance, angle, and error calculations; ABSORB (Coppens, Edwards, and Hamilton), absorption correction calculation; ORTEP (Johnson) figure plotting; HYDROGEN (Trueblood), calculation of hydrogen atomic positions. All calculations were performed on a DEC VAX 11/750 computer. Scattering factors and corrections for anomalous dispersion were taken from the following: *International Tables for X-ray Crystallography*; Kynoch Press: Birmingham, England, 1974; Vol. 10.

(21) $R = (\sum|F_o - F_c|/\sum|F_o|)$; $R_w = (\sum w|F_o - F_c|^2/\sum w|F_o|^2)^{1/2}$, where F_o and F_c are observed and calculated structure factors, respectively, and $w = 1/\sigma^2(F_o)$.

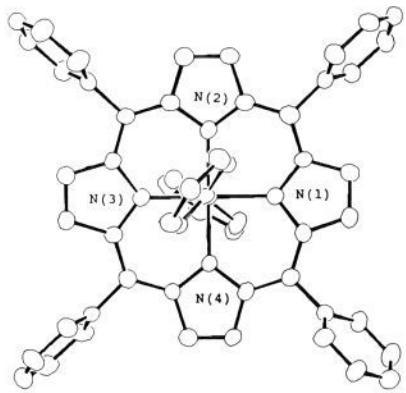

Figure 2. A view of $[Fe(TPP)(py)_2]^+$ down the porphyrin normal indicating axial ligand orientation. The pyridine ligand containing the N(5) atom lies below the porphyrin plane.

Table II. Selected Interatomic Distances (Å) and Selected Bond Angles (deg) for $[Fe(TPP)(py)_2]ClO_4 \cdot 2THF$

N(1)–Fe(1)	1.986 (5)	N(4)–Fe(1)	1.982 (4)
N(2)–Fe(1)	1.988 (5)	N(5)–Fe(1)	2.005 (5)
N(3)–Fe(1)	1.972 (5)	N(6)–Fe(1)	2.001 (5)
N(1)–Fe(1)–N(2)	89.53 (19)	N(3)–Fe(1)–N(5)	88.78 (19)
N(1)–Fe(1)–N(5)	93.15 (19)	N(3)–Fe(1)–N(6)	87.66 (19)
N(1)–Fe(1)–N(6)	90.41 (19)	N(4)–Fe(1)–N(1)	90.00 (19)
N(2)–Fe(1)–N(5)	91.13 (19)	N(4)–Fe(1)–N(2)	179.44 (19)
N(2)–Fe(1)–N(6)	89.38 (18)	N(4)–Fe(1)–N(5)	88.60 (19)
N(3)–Fe(1)–N(1)	178.07 (19)	N(4)–Fe(1)–N(6)	90.91 (19)
N(3)–Fe(1)–N(2)	90.61 (19)	N(6)–Fe(1)–N(5)	176.40 (19)
N(3)–Fe(1)–N(4)	89.88 (19)		

The largest peaks in the final Fourier map were located near the disordered species ($\sim$1.0 e/Å^3).

EPR Measurements. All EPR measurements were made with a Bruker ER200D spectrometer equipped with an Oxford EPR-900 continuous flow cryostat. The magnetic field was calibrated with a NMR gaussmeter, and the frequency was measured with a frequency meter. Crystals were mounted in random orientations on quartz rods and sealed in EPR tubes purged with helium. The crystal orientations were determined at room temperature on a Huber diffractometer. The sample was transferred to the EPR spectrometer where g values were measured as a function of rotation about the rod axis at 6 (2) K.

Details of the single-crystal EPR analysis are described elsewhere.[22-24] The analysis was modified to allow accurate extraction of g values for the case where the three rotation axes are coplanar.[25] Each crystal yielded two sets of EPR data, a consequence of the 2-fold crystallographic symmetry of each sample. A minimum of three data sets are required for determination of the **g** tensor.

Four crystals were used in the determination of the **g** tensor for the $(CN)_2$ complex and three for the (CN)(py) complex. Only two crystals were used in the determination of the **g** tensor for the $(py)_2$ complex. This determination was difficult because the crystals tend to fracture below 80 K. Only three of the four data sets gave adequate fits of g^2 vs rotation angle.

Crystals of the $(CN)_2$ complex gave two pairs of minor signals in addition to the pair of signals used in the analysis reported herein. The **g** tensors of those signals, characterized by a large rhombicity, will be reported in a future publication.

Results and Discussion

Structural Analysis of $[Fe(TPP)(py)_2]ClO_4 \cdot 2THF$ at 128 K. The structure and numbering system for the $[Fe(TPP)(py)_2]$ cation are shown in Figure 1. Figure 2 displays the orientation of the axial ligands with respect to the porphyrin as viewed down the porphyrin normal. Selected bond lengths and bond angles can

(22) Byrn, M. P.; Strouse, C. E. *J. Magn. Reson.* **1983**, *53*, 32.

(23) Byrn, M. B.; Katz, B. A.; Keder, N. L.; Levan, K. R.; Magurany, C. J.; Miller, K. M.; Pritt, J. W.; Strouse, C. E. *J. Am. Chem. Soc.* **1983**, *105*, 4916.

(24) Soltis, S. M.; Strouse, C. E. *J. Am. Chem. Soc.* **1988**, *110*, 2824.

(25) Quinn, R.; Valentine, J. S.; Byrn, M. P.; Strouse, C. E. *J. Am. Chem. Soc.* **1987**, *109*, 3301.

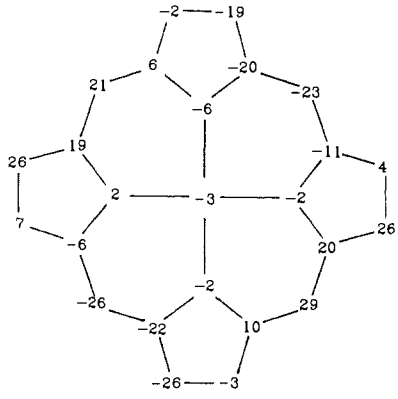

Figure 3. A diagram displaying the ruffling of the porphinato core. The core has the same orientation as that of Figure 2. Atom displacements, in units of 0.01 Å, are measured from the mean plane of the porphinato core.

be found in Table II, and final atomic parameters can be found in Table III.

The four independent Fe–N(pyrrole) bond lengths are essentially equivalent. The average Fe–N(pyrrole) bond length of 1.982 (6) Å is typical of low-spin iron(II) tetraphenylporphyrin complexes.[26] The axial pyridine ligands have essentially equivalent Fe–N bond distances. The average Fe–N(py) bond distance of 2.003 (7) Å is significantly shorter than that of low-spin Fe^{III}(TPP)(CN)(py) (vide infra). The angle between the Fe–N(py) vector and the porphyrin normal is ca. 3° and 2° for N(5) and N(6), respectively. The N(5)–Fe–N(6) bond angle is 176°. Both pyridine rings are tilted approximately 10° from the porphyrin normal.

The angle ϕ, measured between the Fe–N(1) vector and the projection of the pyridine ligand in the plane of the porphyrin, is ca. 52° for the N(6) ligand and ca. 146° for the N(5) ligand, giving rise to idealized D_{2d} symmetry. Figure 3 displays the atomic displacements from the least-squares plane through the porphyrin core. The maximum displacement from the core is 0.29 Å and the average displacement is 0.14 Å. The iron atom is 0.03 Å out of the plane toward the N(5) atom. The porphyrin ligand is S_4 ruffled in such a way as to minimize steric interactions with the pyridine ligands. The average distance between the porphyrin methine carbon atoms and the nearest hydrogen atoms of the pyridine ligands is ca. 2.85 Å. A similar ruffling has been observed by Scheidt et al.[27] in [Fe(TPP)(2-methylimidazole)$_2$]ClO_4.

The Structures of Fe(TPP)(py)(CN) and K[Fe(TPP)(CN)$_2$]. Figure 4 includes schematic representations of these structures as reported by Scheidt, Hatano, and co-workers.[17,18] In the $(CN)_2$ complex the porphyrin ligand is essentially planar and the Fe–C–N bond angle is reported to be 177.8 (3)°, giving rise to nearly perfect axial symmetry. In the (CN)(py) complex the Fe–C–N bond angle is 176.8 (3)° and the ϕ for the pyridine ligand is ca. 41°. The Fe–N(py) bond length of 2.075 (3) Å is significantly longer than the average length of 2.003 (7) Å observed for the $(py)_2$ complex, and the Fe–C(CN) bond length of 1.908 (4) Å is significantly shorter than the 1.975 (2) Å length observed for the $(CN)_2$ complex. The difference in Fe–C(CN) bond lengths may result in part from the fact that in the $(CN)_2$ complex the nitrogen atoms of the cyanide ligands coordinate the potassium counterions and in part from the repulsion between the negatively charged cyanide ions. The longer Fe–N(py) distance in the (CN)(py) complex must be attributed to a trans influence.

Single-Crystal EPR Analysis. The Crystal Field and Spin–Orbit Coupling. Taylor[28] has provided an elegant analysis of the **g** tensor of low-spin d^5 systems. For ferric porphyrin complexes the spin–orbit and crystal field energies are comparable in magnitude

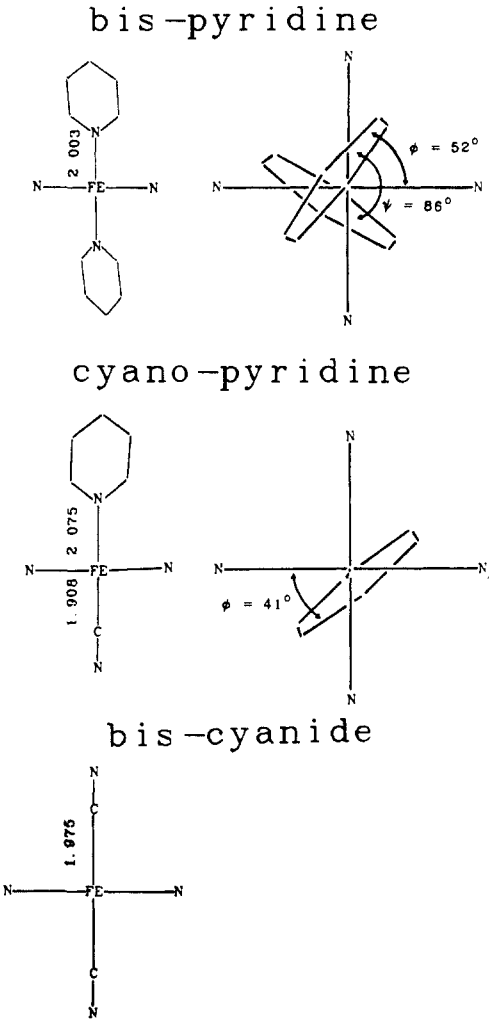

Figure 4. Schematic representations of the $(py)_2$, (CN)(py), and $(CN)_2$ complexes of Fe(TPP) displaying ligand orientation. Only the nitrogen atoms of the porphyrin ligand have been included. Axial views are shown on the right. The axial views are displayed such that the porphyrin nitrogen atom to the right is N(1), on the top is N(2), etc...., as previously labeled.[17,18]

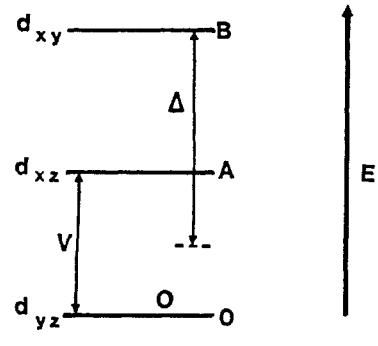

Figure 5. The energy level diagram for a d^5 low-spin porphyrin system. Labels on the three states refer to the identity of the half-filled orbital for a system with orthorhombic symmetry.

and much larger than typical Zeeman energies. Thus wave functions based on combined crystal field and spin–orbit Hamiltonian can be used in conjunction with the Zeeman Hamiltonian to calculate EPR g values.

Taylor showed that in the hole model the wave function for the Kramers doublets can be written as

$$|+\rangle = a|d_{yz}+\rangle - ib|d_{xz}+\rangle - c|d_{xy}-\rangle$$
$$|-\rangle = -a|d_{yz}-\rangle - ib|d_{xz}-\rangle - c|d_{xy}+\rangle \quad (1)$$

where a, b, and c are real. Eigenfunctions of the crystal field and

(26) Scheidt, W. R.; Reed, C. A. *Chem. Rev.* **1981**, *81*, 543.
(27) Scheidt, W. R.; Kirner, J. F.; Hoard, J. L.; Reed, C. A. *J. Am. Chem. Soc.* **1987**, *109*, 1963.
(28) Taylor, C. P. S. *Biochim. Biophys. Acta* **1977**, *491*, 137.

Table III. Positional Parameters for $[Fe(TPP)(py)_2]ClO_4 \cdot 2THF$

atom	X/a	Y/b	Z/c	atom	X/a	Y/b	Z/c
C(1)	0.1439 (3)	−0.0580 (3)	0.1177 (2)	C(44)	0.2708 (3)	−0.1247 (4)	0.0787 (3)
C(2)	0.1038 (3)	−0.1146 (3)	0.0893 (2)	C(45)	0.1479 (3)	−0.0151 (3)	0.2465 (2)
C(3)	0.0474 (3)	−0.0910 (4)	0.0873 (2)	C(46)	0.1498 (3)	−0.0425 (4)	0.2934 (3)
C(4)	0.0513 (3)	−0.0168 (3)	0.1129 (2)	C(47)	0.1397 (3)	0.0084 (4)	0.3303 (3)
C(5)	0.0018 (3)	0.0300 (4)	0.1148 (2)	C(48)	0.1259 (3)	0.0860 (4)	0.3173 (2)
C(6)	0.0069 (3)	0.1057 (3)	0.1338 (2)	C(49)	0.1234 (3)	0.1089 (3)	0.2691 (2)
C(7)	−0.0439 (3)	0.1583 (4)	0.1316 (2)	C(50)	0.1062 (3)	0.1531 (4)	0.0616 (2)
C(8)	−0.0209 (3)	0.2288 (3)	0.1492 (2)	C(51)	0.1101 (3)	0.1945 (4)	0.0188 (2)
C(9)	0.0428 (3)	0.2211 (3)	0.1631 (2)	C(52)	0.1634 (3)	0.2320 (4)	0.0172 (2)
C(10)	0.0810 (2)	0.2809 (3)	0.1834 (2)	C(53)	0.2111 (3)	0.2255 (4)	0.0571 (2)
C(11)	0.1426 (3)	0.2709 (3)	0.1997 (2)	C(54)	0.2041 (3)	0.1836 (3)	0.0979 (2)
C(12)	0.1825 (3)	0.3310 (3)	0.2241 (2)	O(5)	0.7116 (3)	0.4592 (4)	0.1078 (3)
C(13)	0.2369 (3)	0.2981 (3)	0.2391 (2)	C(55)	0.7265 (5)	0.4801 (6)	0.0612 (4)
C(14)	0.2322 (2)	0.2168 (3)	0.2228 (2)	C(56)	0.7069 (5)	0.5648 (6)	0.0513 (4)
C(15)	0.2790 (3)	0.1636 (3)	0.2310 (2)	C(57)	0.6767 (5)	0.5848 (6)	0.0910 (4)
C(16)	0.2745 (2)	0.0900 (3)	0.2098 (2)	C(58)	0.6869 (5)	0.5213 (7)	0.1303 (4)
C(17)	0.3242 (3)	0.0365 (3)	0.2126 (2)	N(1)	0.1102 (2)	0.0032 (3)	0.1316 (2)
C(18)	0.3043 (3)	−0.0249 (3)	0.1825 (2)	N(2)	0.0590 (2)	0.1448 (3)	0.1535 (2)
C(19)	0.2425 (3)	−0.0121 (3)	0.1622 (2)	N(3)	0.1739 (2)	0.2012 (3)	0.1984 (2)
C(20)	0.2050 (3)	−0.0651 (3)	0.1303 (2)	N(4)	0.2242 (2)	0.0581 (3)	0.1789 (2)
C(21)	−0.0587 (3)	−0.0017 (3)	0.0922 (2)	N(5)	0.1345 (2)	0.0616 (3)	0.2333 (2)
C(22)	−0.0845 (3)	−0.0604 (4)	0.1160 (3)	N(6)	0.1520 (2)	0.1480 (3)	0.1014 (2)
C(23)	−0.1400 (3)	−0.0918 (4)	0.0945 (3)	Fe(1)	0.1419 (1)	0.1019 (1)	0.1662 (1)
C(24)	−0.1699 (3)	−0.0655 (4)	0.0484 (3)	Cl(1)	0.1006	−0.1718	0.3958
C(25)	−0.1449 (3)	−0.0078 (4)	0.0235 (3)	O(1)	0.1175	−0.1062	0.4284
C(26)	−0.0892 (3)	0.0239 (4)	0.0454 (3)	O(2)	0.0636	−0.2238	0.4169
C(27)	0.0559 (3)	0.3608 (3)	0.1911 (2)	O(3)	0.1532	−0.2126	0.3896
C(28)	0.0407 (3)	0.4137 (4)	0.1528 (2)	O(4)	0.0680	−0.1445	0.3483
C(29)	0.0195 (3)	0.4884 (4)	0.1612 (3)	Cl(1B)	0.0988	−0.1727	0.3963
C(30)	0.0141 (3)	0.5093 (3)	0.2083 (3)	O(1B)	0.0689	−0.2419	0.4078
C(31)	0.0267 (3)	0.4552 (4)	0.2464 (2)	O(2B)	0.0915	−0.1110	0.4299
C(32)	0.0485 (3)	0.3813 (3)	0.2380 (2)	O(3B)	0.0735	−0.1489	0.3462
C(33)	0.3389 (3)	0.1915 (3)	0.2604 (2)	O(4B)	0.1612	−0.1890	0.4013
C(34)	0.3724 (3)	0.2421 (4)	0.2373 (3)	O(6)	0.5771	0.4292	0.9718
C(35)	0.4273 (3)	0.2701 (4)	0.2640 (3)	C(59)	0.5873	0.3552	0.9531
C(36)	0.4484 (3)	0.2476 (4)	0.3127 (3)	C(60)	0.5645	0.2988	0.9810
C(37)	0.4163 (3)	0.1967 (4)	0.3353 (3)	C(61)	0.5403	0.3378	1.0168
C(38)	0.3604 (3)	0.1669 (4)	0.3086 (2)	C(62)	0.5481	0.4184	1.0111
C(39)	0.2342 (3)	−0.1348 (3)	0.1125 (2)	O(6B)	0.5426	0.2872	1.0100
C(40)	0.2251 (3)	−0.2102 (3)	0.1284 (2)	C(59B)	0.5068	0.3475	0.9850
C(41)	0.2524 (3)	−0.2750 (4)	0.1114 (3)	C(60B)	0.5442	0.4017	0.9686
C(42)	0.2884 (3)	−0.2641 (4)	0.0777 (3)	C(61B)	0.6031	0.3749	0.9835
C(43)	0.2982 (3)	−0.1884 (4)	0.0609 (3)	C(62B)	0.6021	0.3042	1.0091

spin–orbit Hamiltonian can then be obtained from the following equation.

$$(-\lambda)\begin{vmatrix} 0 & i/2 & -1/2 \\ -i/2 & -A & i/2 \\ -1/2 & -i/2 & -B \end{vmatrix}\begin{vmatrix} a \\ -ib \\ -c \end{vmatrix} = E\begin{vmatrix} a \\ -ib \\ -c \end{vmatrix} \quad (2)$$

The diagonal elements of the matrix are the crystal field terms in units of the spin–orbit coupling constant,[29] λ; A and B correspond to the crystal field energies of the d_{xz} and d_{xy} orbitals relative to the d_{yz} orbital (see Figure 5). This equation requires that

$$E/\lambda = -(b + c)/2a$$
$$A = E/\lambda + (a + c)/2b$$
$$B = E/\lambda + (a + b)/2c \quad (3)$$

The principal g values can be expressed in terms of a, b, and c through the relationship

$$g_j = \langle +|(L_j + 2S_j)|+\rangle - \langle -|(L_j + 2S_j)|-\rangle;\ j = x, y, z$$

to yield

$$g_z = 2[(a + b)^2 - c^2]$$
$$g_y = 2[(a + c)^2 - b^2]$$
$$g_x = 2[a^2 - (b + c)^2] \quad (4)$$

(29) The free ion value of the spin–orbit coupling constant, λ, for iron is 420 cm^{-1}, but this value can be significantly reduced with increased covalency (see: Palmer, G. In *Iron Porphyrins*, Part II; Lever, A. B. P., Gray, H. B., Eds.; Addison Wesley: Reading, MA, 1983; pp 43–88).

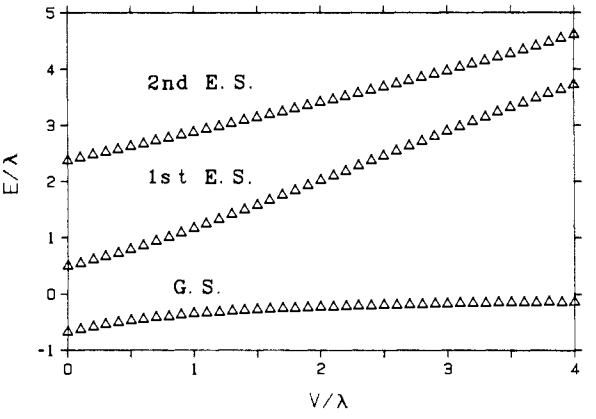

Figure 6. A plot of the relative energies of the lowest three Kramers doublets vs the rhombic splitting for an axial splitting of 2.2λ.

These expressions can be rearranged to give the coefficients in terms of the principal g values.

$$a = (g_z + g_y)/[8(g_z + g_y - g_x)]^{1/2}$$
$$b = (g_z - g_x)/[8(g_z + g_y - g_x)]^{1/2}$$
$$c = (g_y - g_x)/[8(g_z + g_y - g_x)]^{1/2} \quad (5)$$

The crystal field energies A and B are obtained by substituting eq 5 into eq 3.

$$A = g_x/(g_z + g_y) + g_y/(g_z - g_x)$$

$$B = g_x/(g_z + g_y) + g_z/(g_y - g_x) \quad (6)$$

The crystal field parameters are defined as shown in Figure 5; $V = A$, $\Delta = B - A/2$.

Of particular interest in the present investigation is the behavior of the wave functions, the energies, and the g values in the limit of axial symmetry. Figures 6, 7, and 8 are based on a solution of eq 2 with Δ fixed at a value of 2.2λ, the value observed for both the $(py)_2$ and $(CN)_2$ complexes (vide infra).

In Figure 6, a plot of the coefficients of the ground-state wave function vs the rhombic splitting shows that when the rhombic splitting approaches zero, the wave function contains equal contributions from the two out-of-plane real d orbitals. Such a delocalization has a number of significant implications.

In Figure 7 the relative energies of the lowest three Kramers doublets are plotted as a function of the rhombic splitting. In the region where the rhombic splitting is larger than the spin–orbit coupling constant, λ (as observed for most low-spin ferric porphyrin complexes), the energy separation between the ground state and the first excited state is approximately equal to the rhombic splitting, V. In the limit of small V, this separation approaches the spin–orbit coupling constant, λ. The spin–orbit stabilization of the ground state, $\lambda/2$, will be shown to have potential structural consequences.

In Figure 8 the three principal g values are plotted as a function of the rhombic splitting. In the region where V is large, the principal g values are all close to the free electron value. As V becomes smaller, the g values diverge. For rhombic splittings less than ca. 0.5λ, g_x becomes negative. This sign change leads to an ambiguity in the extraction of crystal field parameters from experimentally determined g values, because the sign of the g values is not determined in a conventional EPR experiment.

The g Value Anisotropy. The principal g values obtained in the single-crystal measurements (Table IV) are in reasonable agreement with those obtained from the spectra of polycrystalline samples (where only the maximum g value is accurately measured). Ellipsoidal representations of the **g** tensors are shown in Figure 9. The direction cosines in the molecular coordinate systems are listed in Table V. In all three complexes the largest g value occurs with the magnetic field approximately perpendicular to the porphyrin plane. Each complex displays a significant anisotropy in the porphyrin plane. The principal axes of the in-plane anisotropy are directed along the Fe–N vectors of the porphyrin ligand in the $(CN)_2$ and (CN)(py) complexes, whereas they are directed between porphyrin Fe–N vectors in the $(py)_2$ complex. An interpretation of these observations must be based on the crystal field parameters that can be extracted from the principal g values. This requires, however, that the ambiguity regarding the sign of g_x be resolved.

The Sign of g_x. In all three of these HALS complexes, the sign of g_x (or more precisely, the sign of the product of the three principal g values) is ambiguous. Table IV gives crystal field parameters calculated for both positive and negative assignments.

Huynh, Emptage, and Münck[30] showed that the sign of the product of the three principal g values can be determined from magnetic Mössbauer spectra. Rhynard, Lang, and co-workers[31] used magnetic Mössbauer measurements of frozen solutions to determine the crystal field parameters of $[Fe^{III}PPIX(py)_2]Cl$; this analysis gave $\Delta = 1.66\lambda$ and $V = 0.22\lambda$, and a covalency parameter $k = 1.08$. On the basis of eq 2, which ignores covalency effects, these values of V and Δ give calculated principal g values of −0.53, 1.33, and 3.49. The correspondence between the magnitudes of these principal g values and those obtained herein for the [Fe(TPP)(py)$_2$] cation ($|g_x| = 0.46$, $|g_y| = 1.12$, $|g_z| = 3.70$) indicates a negative assignment of g_x for the $(py)_2$ complex.[32]

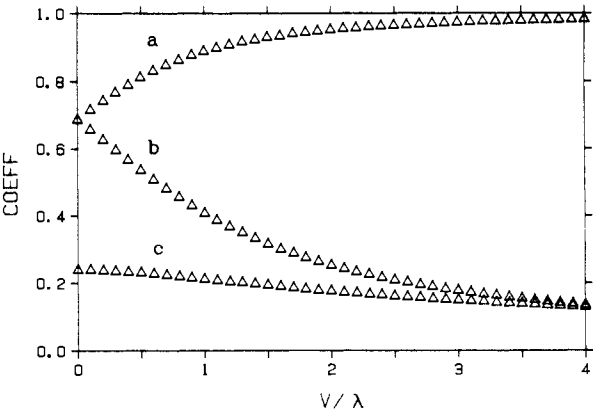

Figure 7. A plot of the coefficients of the ground-state wave function vs the rhombic splitting (Δ fixed at 2.2λ).

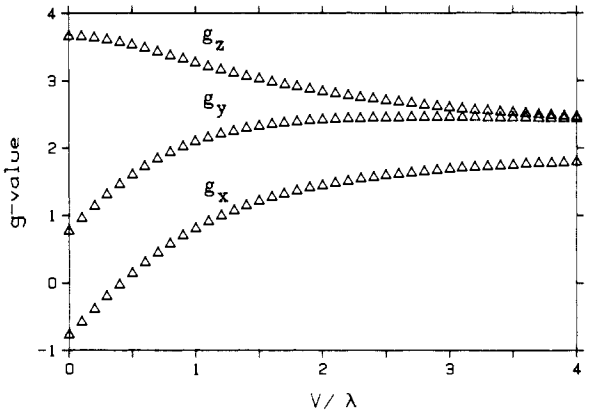

Figure 8. A plot of the three principal g values vs the rhombic splitting for an axial splitting of 2.2λ.

Buttressing this argument is the fact that the Δ based on the negative assignment of g_x is 2.2λ, while that based on the positive assignment is 5.5λ. Pyridine should be a weaker π donor than imidazole,[33] and hence should give a Δ smaller than the average value of ca. 3.1λ observed for bis(imidazole) complexes.[24]

A similar argument can be applied to the assignment of the $(CN)_2$ complex. A study[33] of the ligand-to-metal charge-transfer spectra of Fe(III) complexes indicates that both pyridine and cyanide are poorer π donors than imidazole. In this case a negative assignment of g_x gives a Δ of 2.2λ while a positive assignment gives a Δ of 6.9λ, again indicating that the negative assignment is correct.

The choice of the sign of g_x for the (CN)(py) complex is more ambiguous. In this case a negative assignment gives $\Delta = 1.30\lambda$ while a positive assignment gives $\Delta = 2.1\lambda$. Since one can reasonably expect the Δ of the (CN)(py) complex to be approximately intermediate between those of the $(CN)_2$ and $(py)_2$ complexes, the positive assignment might appear to be favored in this case, giving Δ's for all three complexes close to 2λ. However, the significant trans influence observed in this complex could result in nonlinear behavior of the crystal field parameters. Fortunately, the magnitude of g_x is sufficiently small in this case that the ambiguity does not make a large difference in the magnitudes of the crystal field parameters obtained.

Chemical Consequences of Orbital Degeneracy and Spin–Orbit Coupling. The large g value anisotropy observed in the EPR spectra of these complexes results from the fact that the rhombic splitting is small compared to the spin–orbit coupling constant.

(30) Huynh, B. H.; Emptage, M. H.; Münck, E. *Biochim. Biophys. Acta* **1978**, *534*, 295.
(31) Rhynard, D.; Lang, G.; Spartalian, K.; Yonetani, T. *J. Chem. Phys.* **1979**, *71*, 3715.
(32) Rhynard et al. also analyzed the magnetic Mössbauer spectra of $Fe^{III}PPIX(py)(CN)$ and $[Fe^{III}PPIX(CN)_2]^-$. However, in the analysis of the (py)(CN) complex, the crystal field parameters were constrained to those calculated for cyanomyoglobin assuming a positive g_x. In the case of the $(CN)_2$ complex, the crystal field parameters were constrained to values based on what appears to be an incorrect assignment of the EPR spectrum.
(33) Johnson, C. R.; Shepard, R. E. *Inorg. Chem.* **1983**, *22*, 3506.

Table IV. Electronic Parameters for HALS Complexes[a]

	g_z	g_y	g_x	Δ	V	V/Δ	$(a^2 + b^2 + c^2)$
bis(pyridine)	3.70	1.12	0.46	5.5	0.44	0.08	0.98
			−0.46	2.2	0.17	0.08	1.03
cyano pyridine	3.31 (2)	1.76 (4)	0.34 (4)	2.1 (1)	0.66 (1)	0.32 (2)	0.97
			−0.34 (4)	1.30 (1)	0.42 (2)	0.32 (2)	1.00
bis(cyanide)	3.70 (3)	1.05 (3)	0.52 (2)	6.87 (6)	0.44 (1)	0.064 (3)	0.98
			−0.52 (2)	2.18 (7)	0.14 (1)	0.064 (3)	1.02

[a] The crystal field parameters are given in terms of the spin–orbit coupling constant.

Table V. Direction Cosines of the Principal Axes of the **g** Tensor in the Molecular Coordinate System

|g|	x'	y'	z'
	Bis(pyridine)		
0.46	−0.626 60	−0.773 84	0.076 72
1.12	−0.778 24	0.627 96	−0.015 71
3.70	−0.040 13	−0.074 98	−0.996 49
	Cyano Pyridine		
0.34	0.085 82	0.981 32	0.172 19
1.76	0.977 16	−0.116 63	0.177 63
3.31	−0.194 40	−0.153 01	0.968 92
	Bis(cyanide)		
0.52	0.100 35	0.994 68	0.023 36
1.05	−0.994 90	0.007 68	−0.007 68
3.71	0.009 98	0.022 47	−0.999 70

[a] The axes x', y', and z' are defined in Figure 9.

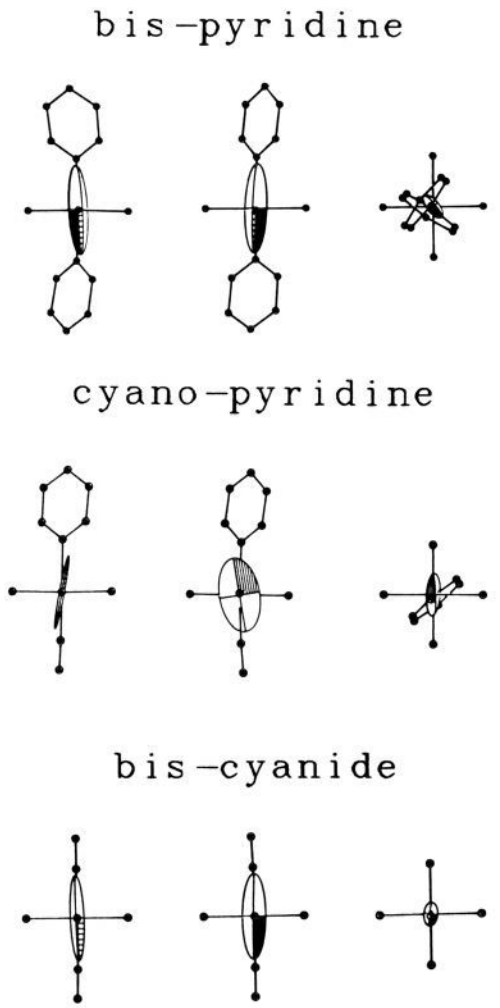

Figure 9. The **g** tensor representation for the $(py)_2$, (CN)(py), and $(CN)_2$ complexes of Fe(TPP). From left to right the molecular x', y', and z' axes point toward the reader. The orientation with z' pointing toward the reader for the $(py)_2$ complex is the same as that in Figure 2 (N(5) lies below the plane of the porphyrin).

Apart from the unusual EPR spectrum, this degeneracy has a number of significant chemical consequences related to spin–orbit mixing of the two out-of-plane d orbitals. (In the limit of small V and large Δ, the wave functions for the ground-state Kramers doublet become eigenfunctions of the spin–orbit Hamiltonian of the form $1/2^{1/2}(|d_{yz}+\rangle - i|d_{xz}+\rangle)$ and $1/2^{1/2}(-|d_{yz}-\rangle - i|d_{xz}-\rangle)$).

One consequence of this mixing is that the pseudo-Jahn–Teller distortion of the porphyrin ligand, associated with the localization of the spin, is greatly reduced in these highly symmetric systems. In a previous series of investigations in this laboratory,[24] it was shown that in localized ferric porphyrin complexes the contribution of such a distortion to the rhombic splitting does not exceed about 0.4λ. Since the spin–orbit stabilization associated with the delocalized state, $\lambda/2$, exceeds the Jahn–Teller stabilization associated with the localized state, $V/2 = 0.2\lambda$, the system adopts a delocalized electronic structure in which the driving force for the distortion disappears.

Another potential consequence of the spin–orbit stabilization involves the molecular geometry of the $(py)_2$ complex. While a large number of bis(imidazole) complexes of ferric porphyrins, both in the crystalline state and in frozen solution, have been shown to adopt a parallel axial ligand geometry, a large number of bis(pyridine) complexes exhibit HALS EPR spectra,[4,8] and thus presumably have perpendicular geometries. While one can argue that this reflects a steric difference between the 5-membered and 6-membered rings of the ligands, one should not ignore the electronic factors that might contribute.

The parallel geometry results in a crystal field stabilization of $V/2$ with respect to the perpendicular geometry. (The preferred orientation with both axial ligands eclipsing the porphyrin nitrogen atoms results in an additional pseudo-Jahn–Teller contribution to the rhombic splitting and hence an additional crystal field stabilization.) Associated with the perpendicular orientation, however, is the spin–orbit stabilization of $\lambda/2$. Thus, if the rhombic crystal field splitting achieved in the parallel geometry is less than λ, this geometry will be unstable with respect to the perpendicular geometry. The lower the π donor strength of the axial ligands, the more likely the complex is to adopt the perpendicular geometry.

In a recent analysis[24] of bis(imidazole) complexes it was found that two imidazole ligands in the parallel orientation contribute ca. 1.5λ to the rhombic splitting. The fact that this is larger than λ is consistent with the observation that these complexes favor the parallel geometry. One cannot measure the individual ligand contributions when the ligands are in the perpendicular geometry. However, it has been found that for ligands with the same donor atom identity and hybridization, V/Δ is nearly constant.[23] On the basis of the axial splitting observed for the bis(imidazole) (Δ ca. 3.1λ) and the $(py)_2$ complexes ($\Delta = 2.2\lambda$), at $|\phi| = 45°$ the contribution to V of two parallel pyridine ligands should be about 1λ. Hence for the $(py)_2$ complex the electronic factors favoring the parallel and perpendicular orientations appear to be approximately equal.

Another consequence of the spin delocalization is that one would expect the electric field gradient tensor to be nearly axial, with the symmetry axis along the porphyrin normal. Ignoring ligand contributions, V_{zz} should be positive. In the Mössbauer investigation of $[Fe^{III}PPIX(py)_2]^+$, Rhynard et al.[31] found that the electric field gradient of largest magnitude corresponds to the porphyrin normal and that this gradient is positive. They also, however, found significant EFG anisotropy in the porphyrin plane. In "normal" low-spin ferric porphyrin complexes, in which the

spin is localized in a single out-of-plane real d orbital, the maximum EFG should be negative and correspond to the normal of the half-filled orbital (and hence lie in the porphyrin plane). A single-crystal Mössbauer investigation by Harami[34] showed that this was indeed the case for the azide complex of myoglobin.

In-Plane *g* Anisotropy. In these nearly axial systems, small changes in the rhombic splitting can have a significant effect on the *g* value anisotropy. While the orientation of the observed in-plane *g* value anisotropy of the two symmetrically ligated complexes is dramatically different (see Figure 9), the difference in the crystal fields is very small. The alignment of the principal axes of the **g** tensor with the Fe–N vectors of the porphyrin in the $(CN)_2$ complex could be the result of a small lattice-induced distortion of the porphyrin. On the basis of previous investigations,[24] one can estimate that a difference in Fe–N bond distances on the order of 0.01 Å is sufficient to account for the observed rhombic splitting. Similarly, a very slight lattice-induced difference between the two axial pyridine ligands in the $(py)_2$ complex would be sufficient to account for the alignment of the principal axes of the **g** tensor which approximately bisect the Fe–N vectors of the porphyrin. It is not possible to observe either of these distortions directly. In the case of the $(CN)_2$ complex the presence of additional species in the lattice complicates the interpretation of the structural results, and in the case of the $(py)_2$ a phase transition precludes the collection of crystallographic data at low temperature.

Depending on the above assignment of the sign of g_x, the rhombic splitting for the (py)(CN) complex is 0.66λ or 0.41λ. In either case this corresponds to a ground state that is significantly more localized than those of the symmetrically ligated complexes. Although one might expect the pyridine ligand to localize the spin distribution in this complex, the principal axes of the **g** tensor are more nearly aligned with the Fe–N vectors of the porphyrin than they are with the plane of the pyridine ligand which approximately bisects the Fe–N vectors. This implies that something other than the asymmetry of the pyridine ligand controls the spin distribution and that the asymmetry of the pyridine ligand contributes almost nothing to the observed *V*.

One can easily rationalize a small contribution to *V* from the asymmetry for the pyridine ligand. In the previous section it was estimated that the contribution of an individual pyridine ligand to the rhombic splitting in the $(py)_2$ complex is on the order of 0.5λ. (Of course in this complex the contributions of the two ligands have opposite signs.) Since the Fe–N(py) distance in the (CN)(py) complex is much longer than that in the $(py)_2$ complex, one would expect the contribution of the pyridine ligand to be much less than 0.5λ.

Distortion of the porphyrin ligand in highly localized cationic complexes has been found to contribute about 0.4λ to the rhombic splitting;[24] in this less localized complex a smaller contribution would be expected. It would appear that there is some additional contribution to the rhombic splitting of the (CN)(py) complex. Figure 9 shows that both the cyanide ligand and the pyridine ligand are displaced from the porphyrin normal toward N(4). This distortion should tend to raise the energy of the out-of-plane orbital aligned with N(2) and N(4) and localize the spin in this plane. Consistent with this localization, the average Fe–N bond distance in this direction is 0.02 Å longer than the average distance in the orthogonal direction. This difference, which is comparable to values observed in more completely localized complexes,[24] has been shown to be on the order of the difference one would estimate from the spectroscopically determined values of dV/dQ and the metal–nitrogen force constant (see ref 24).

Conclusions

Use of single-crystal measurements has circumvented the problems of obtaining accurate *g* values for nearly axially symmetric ferric porphyrin complexes from polycrystalline or frozen solution samples. Extraction of crystal field parameters from the "highly anisotropic" *g* values of these species, however, requires resolution of an ambiguity concerning the sign of the product of the three principal *g* values. It was demonstrated in a series of three determinations that this resolution can be accomplished in some cases by reference to the axial splittings of related materials. The spin distribution in these axially symmetric ferric porphyrin complexes is governed by spin–orbit interactions which serve to delocalize the spin over the two out-of-plane real d orbitals. This spin–orbit interaction appears to be sufficient to quench any Jahn–Teller distortion of the porphyrin. This same interaction tends to stabilize the perpendicular geometry of complexes with planar axial ligands.

Acknowledgment. The authors acknowledge the support of the National Institutes of Health (GM35329) and the National Science Foundation (CHE 8706780).

Registry No. $[Fe(TPP)(py)_2]ClO_4 \cdot 2THF$, 115269-81-3; $K[Fe(TPP)(CN)_2] \cdot 2$ acetone, 73946-21-1; $Fe(TPP)(CN)(py) \cdot H_2O$, 85135-21-3.

Supplementary Material Available: Tables of anisotropic temperature factors for $[Fe(TPP)(py)_2]ClO_4 \cdot 2THF$ and hydrogen positional parameters (5 pages); listing of structure factors for $[Fe(TPP)(py)_2]ClO_4 \cdot 2THF$ (41 pages). Ordering information is given on any current masthead page.

(34) Harami, T. *J. Chem. Phys.* **1979**, *71*, 1309.